

Comparing Simulated and Observed Particle Energy Distributions through Magnetic Reconnection in Earth's Magnetotail

Nadja Reisinger ¹ and Fabio Bacchini ^{1,2}

¹Centre for mathematical Plasma Astrophysics, Department of Mathematics, KU Leuven, Leuven, Belgium

²Royal Belgian Institute for Space Aeronomy, Solar-Terrestrial Centre of Excellence, Uccle, Belgium

Key Points:

- First time using observations for simulation setups to study particle energization
- Quantitative agreement of the energy spectra between simulation and in-situ measurements in Earth's magnetotail
- Reproduction of the very-high-energy part of the electron energy distribution requires a more realistic simulation

Corresponding author: Nadja Reisinger, nadja.reisinger@kuleuven.be

Abstract

Magnetic reconnection is an explosive process that accelerates particles to high energies in Earth’s magnetosphere, offering a unique natural laboratory to study this phenomenon. We performed fully kinetic 2D simulations of a reconnection event observed by the Magnetospheric Multiscale mission and compared the resulting ion and electron energy distributions with observations. The simulations capture the overall shape and evolution of non-thermal energy distributions for both species, but generally underestimate the very-high-energy tail of the electron spectrum. Variations in numerical parameters have negligible effects on the resulting spectra, while the initial upstream temperatures instead play a critical role in reproducing the observed distributions. This work presents a novel analysis of particle acceleration in fully kinetic modeling of reconnection directly informed by observed, realistic parameters; highlights the limitations of 2D simulations and underlines the need for more realistic simulations (e.g. employing 3D setups) to capture the observed particle energization more accurately.

Plain Language Summary

Magnetic reconnection is a fundamental and powerful plasma-physical process that rapidly releases stored magnetic energy and accelerates charged particles (such as electrons and ions) to high energies. This phenomenon occurs near Earth and in many other astrophysical environments across the universe, often far away and difficult to observe directly. The magnetospheric environment around Earth offers a unique opportunity to study reconnection up close, but satellites can only capture short moments during the whole process. To study reconnection over longer timescales, computer simulations that model both ion and electron behavior can be used. Our simulations are initialized by using satellite measurements from a reconnection event observed in the nightside region of Earth’s magnetic environment to assess how well the computational models reproduce the observed particle energies. We find that the models match the overall features of the observations, which provides a first confirmation that data-inspired simulations can reproduce observed results. Our calculations however do not yet capture the very-high-energy part of the electron population; this indicates that three-dimensional models may be needed to better reproduce the observed particle energies.

1 Introduction

Magnetic reconnection (MR) is a ubiquitous plasma process occurring in many space and astrophysical environments. During reconnection, the topology of the local magnetic field is rapidly rearranged, and magnetic energy is converted into kinetic particle energy, potentially leading to significant particle acceleration (e.g. Yamada et al., 2010). The dominant mechanisms for particle acceleration during MR are Fermi acceleration, betatron acceleration, and direct acceleration by the parallel electric field (e.g. Northrop, 1963; Birn et al., 2012; Dahlin, 2020; Li et al., 2021), while the relative contribution of each mechanism depends on the ambient plasma conditions (Oka et al., 2023). Fermi acceleration is caused by the bouncing of particles between contracting magnetic mirror points or by an encounter with an evolving, curved magnetic field, due to the conservation of the second adiabatic invariant. Betatron acceleration acts in the direction perpendicular to the magnetic field and is driven by increasing magnetic-field strength due to the conservation of the first adiabatic invariant. In contrast, direct acceleration occurs along the magnetic field and results in energy gain through parallel electric fields. An important feature of particle acceleration often associated with MR is the formation of a nonthermal power-law tail in the energy distribution $f \propto E^{-p}$, with E the particle energy and p a spectral index determined by the local plasma conditions. Nonthermal particle spectra associated with MR were observed in numerical simulations with broadly varying physical parameters, ranging from trans- and ultrarelativistic conditions

in astrophysical scenarios (e.g. Sironi & Spitkovsky, 2014; Guo et al., 2014) to nonrelativistic regimes, relevant for e.g. solar flares (e.g. Li, Guo, Li, Stanier, & Kilian, 2019; Zhang et al., 2021).

Compared to other, more distant astrophysical objects, the day- and nightside of Earth’s magnetosphere offers a unique opportunity for in-situ measurements of magnetic reconnection and associated particle dynamics. Especially with the launch of NASA’s Magnetospheric Multiscale (MMS) mission (Burch et al., 2016) in 2015, measurements of plasma parameters at high spatial and temporal resolutions became available to study the microphysics of MR. Furthermore, due to the relatively simple magnetic-field configuration in Earth’s magnetotail, numerous reconnection events observed in that region have been used to study the associated particle acceleration (e.g. Øieroset et al., 2002; R. Ergun et al., 2018; R. E. Ergun et al., 2020; Cohen et al., 2021; Oka et al., 2022; Rajhans et al., 2025). However, relatively few fully kinetic simulations (i.e. including the electron physics) representing Earth’s magnetotail have been presented in literature (e.g. Lapenta et al., 2020), and most studies have instead focused on reconnection under conditions typical of solar flares (e.g. Li, Guo, & Li, 2019; Li, Guo, Li, Stanier, & Kilian, 2019; Li et al., 2015). Notably, T. K. M. Nakamura et al. (2018) performed a simulation in which the necessary input parameters to set up the initial state were extracted from an observed reconnection event in Earth’s magnetotail. In this study, virtual spacecraft probes were used to compare field data, temperatures, and densities with in-situ satellite measurements, showing remarkable agreement. However, no comparison was made between the simulation and observational data on particle energetics and acceleration. In fact, a quantitative comparison of energy distributions and their evolution between simulations and observations has not yet been performed.

In this study, we carry out a number of fully kinetic simulations initialized with data from an observed magnetotail reconnection event, and focus on evaluating how our runs can reproduce the measured energy distribution of electrons and ions. We perform a parameter study to explore how variations in plasma temperatures and simulation set-up affect the resulting particle energization.

2 Methodology

2.1 Observational Data

In 2015, NASA’s MMS mission (Burch et al., 2016) was launched to study MR on kinetic scales at the Earth’s magnetosphere within two distinct regions: at the dayside magnetopause and in the nightside magnetotail. During the second phase, when the MMS mission was investigating the Earth’s magnetotail, the MMS spacecraft crossed an electron diffusion region (EDR) on July 11, 2017 at 22:34:03 during a reconnection event (e.g. T. K. M. Nakamura et al., 2018; Torbert et al., 2018; Genestreti et al., 2018; R. Nakamura et al., 2019). Our study uses publicly available level-2, burst-mode data from MMS3 during 22:33 - 22:35 UT. The particle data comes from the Fast Particle Detector (FPI; Pollock et al., 2016) and the Energetic Particle Detector (EPD), specifically from the Fly’s Eye Energetic Particle Sensor (FEEPS; Mauk et al., 2016a) and Energetic Ion Spectrometer (EIS; Mauk et al., 2016b). The temperature data and low-energy ranges for both species are from FPI, while EIS and FEEPS cover the high-energy ranges for ions and electrons, respectively. The energy data used in Section 3.3 is averaged during the time window for each energy level, and similar to previous studies (e.g. Oka et al., 2022), only energies higher than 100 eV and 500 eV for electrons and ions, respectively, were considered. This removes data that might be impacted by artificial effects and ensures consistent energy ranges in observations and simulations.

2.2 Simulation Setup

For this study, we conducted 2D fully kinetic simulations with the Particle-in-Cell code ECsim/RelSIM (Lapenta, 2017; Bacchini, 2023), which in the nonrelativistic limit conserves energy exactly to machine precision when the time-centering parameter $\theta = 0.5$. The simulations are initialized using a double Harris current sheet (Harris, 1962), where the magnetic field and number density are described by $B_x(y) = B_0 \tanh(y/\delta)$ and $n_{i,e}(y) = n_d \text{sech}(y/\delta)$, respectively, with B_0 the background magnetic field, δ the half-thickness of the initial current sheet, and n_d the plasma number density in the current sheet. The upstream plasma is initialized with uniform temperature and density as described below. Our simulations use periodic boundary conditions along both axes and a small initial perturbation to expedite the onset of MR. All simulation setups discussed below are based on the MR event observed on July 11, 2017, which was previously studied with fully kinetic simulations by T. K. M. Nakamura et al. (2018). In that work, a notable agreement was found between fluid plasma quantities measured by virtual spacecraft probes in the simulations and the MMS3 observation. In the same spirit, the input parameters used in our runs are taken from observational data and are represented in Table 1, which provides a summary of all the runs we performed.

Simulation *R0* serves as the reference run and is based on the input parameters from T. K. M. Nakamura et al. (2018) without major modifications, except for the omission of the guide field, whose strength is 3% of the upstream field and is therefore neglected. For the upstream magnetic-field strength (B_0), density (n_0) and ion and electron temperatures ($T_{0,i}$ and $T_{0,e}$) the following values are used: $B_0 = 12$ nT, $n_0 = 0.3$ cm⁻³, $T_{0,i} = 1500$ eV, and $T_{0,e} = 500$ eV. Furthermore, the initial density (n_d) and ion and electron temperatures ($T_{d,i}$ and $T_{d,e}$) in the current sheet are given by $n_d/n_0 = 3$, $T_{d,i}/T_{0,i} = 3$, and $T_{d,e}/T_{0,e} = 3$. These values are based on MMS3 observations from the 11 July 2017 event at 22:32–22:34 UT; for a detailed explanation of the parameter selection, see T. K. M. Nakamura et al. (2018). The simulation box spans $L_x \times L_y = 23 \times 69(d_{0,i})^2$ with a grid spacing $\Delta x = \Delta y = 0.12d_{0,i}$, where $d_{0,i}$ is the ion skin depth calculated with n_0 , and a time step of $0.03\Omega_{0,i}^{-1}$, where $\Omega_{0,i}$ is the ion cyclotron frequency calculated with B_0 . Δx and Δy are chosen such that, at the initial state, each cell resolves at least one electron skin depth, which is $0.125d_{0,i}$ for run *R0* and similarly applied in all other runs. The half-thickness of the current sheet is $\delta = 0.35d_{0,i}$, the ion-to-electron mass ratio is $m_i/m_e = 64$, and in the whole simulation domain, 2.8×10^7 particles are used, which are initialized with a Maxwellian particle distribution.

All other simulations (*R1–R7*) deviate from *R0* in at least one parameter; these variations are highlighted in bold in Table 1. To investigate the influence of the mass ratio m_i/m_e on the particle energization, we set up runs *R1* and *R2*, with $m_i/m_e = 25$ and 100, respectively. Due to the change in m_i/m_e , modifications were made for the grid spacing Δx and the time step Δt to ensure resolving one inertial length of electrons with one cell in the initial simulation state and to keep the ratio $\Delta t/\Delta x$ between 0.2 and 0.25, as in *R0*. For runs *R3*, *R4*, and *R5*, the box size of the simulation domain is varied, while in *R3* and *R4*, L_x or L_y are respectively increased by 25% while keeping the length of the other box side constant. In *R5*, both L_x and L_y are increased by 25%, while all other parameters in these three runs are the same as *R0*. For the last two runs, *R6* and *R7*, the temperatures of the background plasma were modified. Specifically, in *R6* the ion temperature $T_{0,i}$ is kept constant and the electron temperature $T_{0,e}$ is decreased to 150 eV to obtain $T_{0,i}/T_{0,e} = 10$, instead of 3 as in *R0*. Hence, the plasma- β , $\beta = \beta_i + \beta_e = n_0 k 8\pi (T_{0,i} + T_{0,e}) / B_0^2$, was reduced from 0.16 to 0.13 due to the change in $T_{0,e}$. As MMS3 crosses the EDR along the MR exhausts (Torbert et al., 2018), the conditions of the upstream plasma are not exactly known; hence, the temperatures ($T_{0,i}$, $T_{0,e}$) are estimated with a different approach in the last run (*R7*). Thus, for the initial state of the simulation, ion and electron temperatures are obtained by Maxwellian fit to the observations, as we discuss in later sections. This leads to $T_{0,i} = 5100$ eV and $T_{0,e} = 1000$ eV, as

Table 1. Overview of all eight simulations, with deviations from the reference simulation (*R0*) in bold, reporting the mass ratio between ions and electrons m_i/m_e , grid spacing $\Delta x = \Delta y$, time step Δt , domain size $L_x \times L_y$, total plasma- β , background magnetic field B_0 , and electron and ion temperatures $T_{0,e}$ and $T_{0,i}$. Length scales are normalized to the ion inertial length $d_{0,i}$ calculated with the background density n_0 , and time scales are normalized to the inverse ion cyclotron frequency $\Omega_{0,i}^{-1}$ calculated with B_0 .

Run	m_i/m_e	$\Delta x/d_{0,i}$	$\Delta t/\Omega_{0,i}^{-1}$	$L_x/d_{0,i}$	$L_y/d_{0,i}$	β	B_0 [nT]	$T_{i,0}$ [eV]	$T_{0,e}$ [eV]	$T_{0,i}/T_{0,e}$
<i>R0</i>	64	0.12	0.03	23	69	0.16	12	1500	500	3.0
<i>R1</i>	25	0.15	0.03	23	69	0.16	12	1500	500	3.0
<i>R2</i>	100	0.08	0.02	23	69	0.16	12	1500	500	3.0
<i>R3</i>	64	0.12	0.03	29	69	0.16	12	1500	500	3.0
<i>R4</i>	64	0.12	0.03	23	86	0.16	12	1500	500	3.0
<i>R5</i>	64	0.12	0.03	29	86	0.16	12	1500	500	3.0
<i>R6</i>	64	0.12	0.03	23	69	0.13	12	1500	150	10.0
<i>R7</i>	64	0.12	0.03	23	69	0.16	21	5100	1000	5.1

well as to $T_{0,i}/T_{0,e} = 5.1$, and agrees with the median temperature values within the time window: 996 eV for the electron temperature and 5122 eV for the ion temperature. Furthermore, in this run, the magnetic-field strength B_0 is increased to 21 nT to maintain the same plasma- β as in *R0*.

3 Results

3.1 Overview of the Simulation Results

The normalized time evolution of various energy components throughout the simulation *R0* is shown in Figure 1a), and exhibits the typical temporal dynamics of energy transfer during reconnection processes. After around $15\Omega_{0,i}^{-1}$, the total magnetic energy E_{mag} starts to decrease, marking the onset of the nonlinear reconnection phase. This is followed by a gradual increase in the ion kinetic energy $E_{\text{kin},i}$ and subsequently in the electron kinetic energy $E_{\text{kin},e}$ — indicating the conversion of magnetic energy into kinetic particle energy. At around $80\Omega_{0,i}^{-1}$, the rate of depletion of magnetic energy slows significantly, similar to the enhancement in both kinetic energies. The change in total internal energy ΔE_{tot} remains constant throughout the simulation, with only minor deviations that are negligible compared to the changes observed in the other energy components. Notably, this is a unique characteristic of the used code, see Subsection 2.2. All other simulations conducted show the same qualitative behavior in the energy evolution and are therefore not shown here.

Figure 1b) and c) show the evolution of the energy distribution for ions and electrons, respectively, from the same simulation, *R0*. Both species deviate substantially from the initial distribution (dashed lines) over time, as indicated by the darker solid lines representing later simulation times. During the run, both species are energized to higher energies and a nonthermal population appears. Similarly, in the other runs, a deviation from the Maxwellian particle distribution and the appearance of a nonthermal population are always observed.

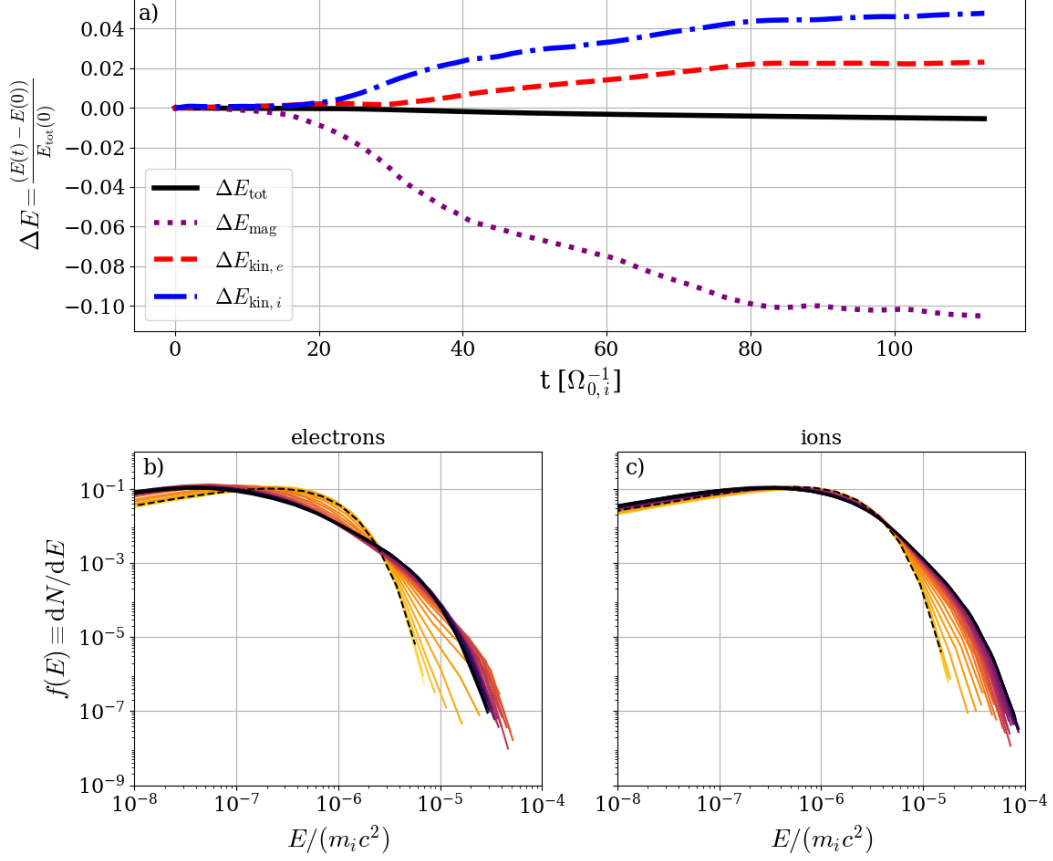


Figure 1. Evolution of different energy quantities throughout the simulation *R0* in a), calculated as the energy change $\Delta E = (E(t) - E(0))/E_{\text{tot}}(0)$, with E the specific energy quantity (e.g. magnetic or kinetic) and E_{tot} the total energy within the system at $t = 0$. Energy distribution of energy $f(E) \equiv dN/dE$ for electrons and ions in panel b) and c), respectively, at different times throughout the same simulation. Darker shades indicate later times. Both panels show the evolution until $t = 105\Omega_{0,i}^{-1}$. The dashed lines show the initial distribution of each particle species.

3.2 Parameter Study

Fully kinetic simulations impose artificial limitations compared to real processes, such as a finite box size or the usage of a reduced ion-to-electron mass ratio. In order to study the influence of these characteristics on the particle energization during MR, certain parameters have been changed in simulations *R1–R7* and compared with the reference simulation *R0*: the mass ratio m_i/m_e , the size of the simulation domain $L_x \times L_y$, and the initial electron temperature $T_{0,e}$ (see Table 1). The electron energy distributions for different simulations are shown in Figure 2a) - c), where the distribution for the initial state ($t = 0$) and at a later stage ($t = 90\Omega_{0,i}^{-1}$) in dashed and solid lines, respectively, are plotted. The normalization of the energy distribution is discussed in Section 3.3. In Figure 2a), the electron energy distributions for different m_i/m_e are shown. In runs *R1* and *R2*, m_i/m_e was varied from 64 (as used in *R0*) to 25 and 100, respectively. Subsequently, the grid spacing and the time steps were adapted in order to resolve at least one electron skin depth per cell at the beginning of the simulation and keep a consistent $\Delta x/\Delta t$ ratio between all simulations, see Table 1. Although there is a minimal tendency to go to larger energies for smaller m_i/m_e , the resulting energy spectra are essentially

insensitive. In Figure 2b), the electron energy distributions for different simulation domain sizes are shown. *R0* is the reference box with $L_x \times L_y = 23 \times 69(d_{0,i})^2$, while in *R3* and *R4*, L_x or L_y are increased by 25%, respectively. In the last run (*R5*) in this subplot, the box size is increased in both directions by 25%, leading to $L_x \times L_y = 29 \times 86(d_{0,i})^2$. The energy distributions for both species show essentially no differences. In our last parameter scan, the initial temperature ratio $T_{0,i}/T_{0,e}$ was enhanced from 3 to 10 (run *R6*), while $T_{0,i}$ was kept at the same initial value as in *R0*. The ion energy distribution shows no difference between the two cases and is thus not shown here. Figure 2c) instead shows the resulting electron energy distribution of the reference simulation *R0* compared with the result of run *R6*. In this case, a clear difference in the energy distribution between the two simulations at $t = 90\Omega_{0,i}^{-1}$ is visible. Notably, a higher $T_{0,i}/T_{0,e}$ (run *R6*) leads to stronger electron energization. Although electrons in run *R6* start at significantly lower energies than in *R0*, their final state reaches energies comparable to those attained in *R0*.

In summary, the numerical parameters m_i/m_e and $L_x \times L_y$ have no essential effect on the resulting energy spectra, supporting the validity of the parameters used in *R0*. In contrast, the upstream particle temperatures must be selected with greater caution due to their significant influence on the particle energization. Accordingly, a different method was used to estimate the upstream temperatures in run *R7* to quantitatively reproduce the measurements, as described below.

3.3 Comparison between Observations and Simulations

The ultimate goal of this study is to compare the particle energization resulting from magnetic reconnection observed at the Earth's magnetotail with the outcome from fully kinetic simulations. One challenging aspect of this comparison is ensuring consistent units and scaling of physical quantities between observations and simulations. Hence, all the energies, from observations and simulations, are normalized by $m_i c^2$ and can also be easily normalized for the different energy ranges from MMS observations. However, the comparison of the energy distributions from both techniques posed additional difficulties, as the units of the differential directional number flux from MMS measurements are challenging to replicate in simulations. Thus, particle fluxes within a certain energy range are normalized by the total number of particles across all energy ranges in both observations and simulations. With these normalization, observations and simulations can be compared directly in a quantitative manner, as shown in Figure 2d) and e), where the solid lines are from run *R7* and circles from observations. Notably, the energy distribution functions in the Figure 1 and Figure 2a) - c) use the same scaling. In Figure 2d) and e) we show the energy distribution functions from the simulation until $135\Omega_{0,i}^{-1}$, because the depletion of magnetic energy is reached at a later time compared to the simulation in Figure 1 or 2a) - c). The initial temperature values for run *R7* in Figure 2d) and e) are based on Maxwellian fits of the observed distributions, represented in the dashed and dotted lines. While the Maxwellian fits are in good agreement with the thermal core measured in the observations, matching the nonthermal part of the observed spectrum requires reconnection to push particles to higher energies. Over the evolution of the simulation, the initially Maxwellian populations develop a nonthermal, high-energy part in their energy distributions. The observed energy range is reached at approximately $50\Omega_{0,i}^{-1}$, and from that point the distributions slowly converge to a final, qualitatively similar state. Considering the distributions throughout the simulation, electrons reach higher energies relative to their initial state and exhibit a broader energy distribution than ions at all times. At $t = 50\Omega_{0,i}^{-1}$, the high-energy electron population ($E/(m_i c^2) \gtrsim 10^{-5}$) contains 5% of the total electron population and contributes to 24% of the total kinetic electron energy, while 6% of the ions are in the high-energy population ($E/(m_i c^2) \gtrsim 4 \times 10^{-5}$) and represent 21% of the total kinetic ion energy.

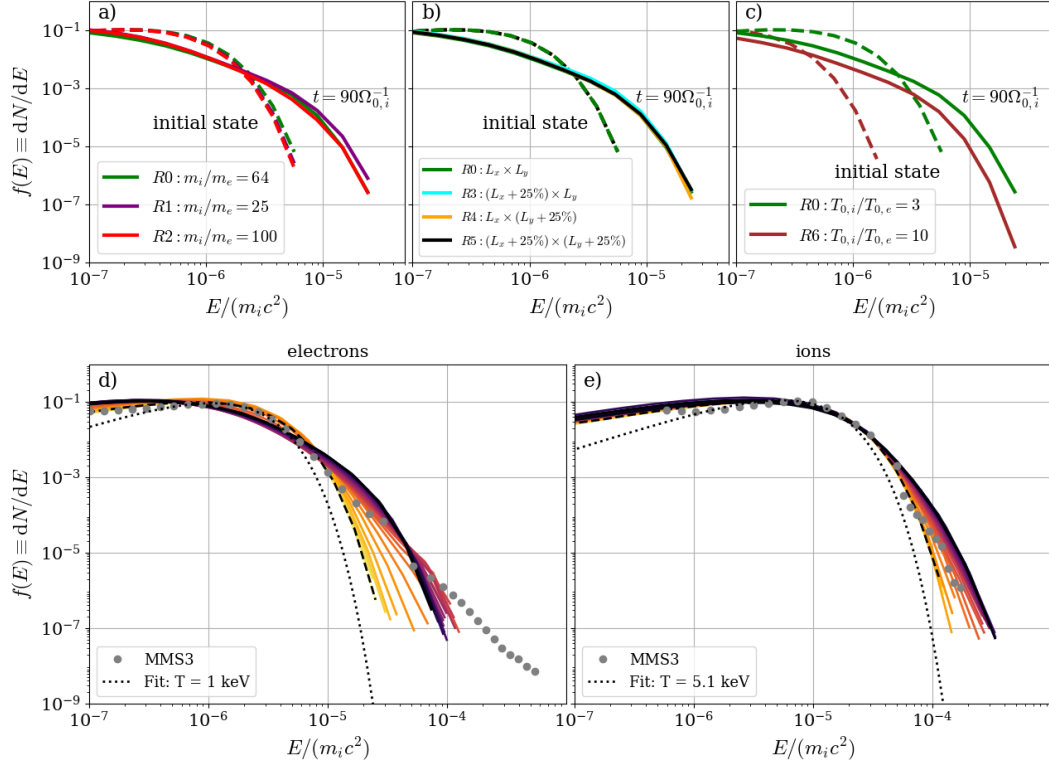


Figure 2. Electron energy distributions for different simulations, considering the variation of specific parameters: the mass ratio m_i/m_e in panel a), the simulation domain size $L_x \times L_y$ in panel b), and the initial temperature ratio $T_{0,i}/T_{0,e}$ in panel c). The solid lines represent the distributions at $t = 90\Omega_{0,i}^{-1}$. Energy distributions from observations and simulation R7 of a reconnection event on 11 July 2017 in Earth’s magnetotail, measured by MMS3 for electrons and ions in panel d) and e), respectively. Electron and ion observational measurements, represented by grey dots, are obtained from the FPI and EPD onboard MMS during 22:33–22:35 UT. Solid lines show the simulated energy distribution for electrons and ions at different simulation times until $135\Omega_{0,i}^{-1}$, with later times shown in darker shades. Dotted lines represent Maxwellian fits with temperatures of 1 keV and 5.1 keV for electrons and ions, respectively. The initial parameters for each run are reported in Table 1. All the dashed lines show the initial energy distribution of the simulation.

For the first time, simulations and corresponding observations of particle energy spectra were directly compared. While our simulations quantitatively retrieve the observed energies and trend for both ions and electrons, the very-high-energy range of electrons remains underrepresented, as discussed in more detail below.

4 Discussions and Conclusions

We performed eight 2D fully kinetic simulations of magnetic reconnection (MR) in Earth’s magnetotail, based on satellite data measured during a reconnection event observed by MMS. While most upstream plasma parameters have been directly inferred from observational data, key numerical parameters of the simulation setup, including mass ratio, box size, as well as the initial temperature ratio, have been systematically varied to assess their effect on the simulated system evolution. For the first time, the electron

and ion energizations resulting from data-inspired fully kinetic simulations were analyzed and directly compared with energy measurements from observations. Overall, our simulations show the development of nonthermal populations in the energy distribution for electrons and ions, attaining energies broadly consistent with those observed in the Earth's magnetotail.

In our parameter scan, we have investigated the effect of the ion-to-electron temperature ratio. While low plasma- β plasma simulations have been performed in previous studies to investigate MR, the focus was primarily on scenarios with equal electron and ion temperatures — conditions that are more appropriate for investigating MR in solar flares (e.g. Li, Guo, & Li, 2019; Li, Guo, Li, Stanier, & Kilian, 2019; Zhang, Guo, Daughton, Li, & Li, 2024), but not representative of Earth's magnetosphere. Our results show a significant influence of the initial particle temperatures on the energization (see Figure 2c)), therefore this distinction is significant.

Our reference simulation (*R0*) is based on the initialization from T. K. M. Nakamura et al. (2018), which demonstrated good quantitative agreement between a virtual spacecraft probe in the simulation and MMS measurements. However, the particle energization in their work did not reproduce the observed energy distributions from MMS3, showing a shift along the x -axis, i.e. energy, due to initial temperatures being too low compared to our final simulation (*R7*). Estimating the upstream plasma conditions is challenging, as the MMS spacecraft crossed the electron diffusion region along the outflow direction, limiting information about the background plasma. Therefore, we initialized the temperature values with a different approach and used a Maxwellian approximation to fit the observations, as shown in Figure 2d) and e). The simulated ion and electron energies are consistent with observations, broadly retrieving the correct ranges for the nonthermal populations.

In our results, the very-high-energy end of the observed electron spectrum, where only a few particles reside, is not accurately captured. This could be attributed to a number of factors, including the rather low number of computational particles used in our simulations. Furthermore, it is generally accepted that in nonrelativistic reconnection scenarios with a low guide field, Fermi-type acceleration dominates particle energization (Dahlin et al., 2017; Li et al., 2018; Li, Guo, Li, Stanier, & Kilian, 2019). This process is driven by curvature drift associated with the relaxation of magnetic tension. In 2D simulations, particles can get trapped in long-lived magnetic islands, because of the limited movement of particles across magnetic field lines (e.g. Jokipii, Kota, & Giacalone, 1993; Jones, Jokipii, & Baring, 1998), which prohibits additional magnetic-field destruction and particle energy gain until primary islands merge with each other (Li et al., 2015, 2017). In more realistic 3D scenarios, particles can initially become confined within flux ropes extending along the out-of-plane direction, until flux-rope kink instabilities are triggered. Flux-rope kinking can destroy these structures and create a more turbulent state, allowing particles to escape and experience additional Fermi acceleration, potentially reaching higher energies (Zhang et al., 2021). To attain more realistic results and capture the very-high-energy end of the electron spectra, in future studies we aim to enhance our simulations by increasing the number of particles, conducting fully 3D simulations to overcome 2D limitations, and considering the conditions for the onset of kink instabilities. Finally, in this study, particle distributions for comparison with observations were measured globally over the whole domain, which is not entirely realistic, as spacecraft data represents localized measurements in space and time. Therefore, future work will include the use of virtual spacecraft probes to enable a more realistic comparison of particle energization between simulations and MMS measurements.

Data Availability Statement

All the observational data used in this study are publicly available at the MMS Science Data Center <https://lasp.colorado.edu/mms/sdc/public/about/browse-wrapper/>. The simulation data of this study are available at <https://doi.org/10.5281/zenodo.17023279>. The simulation results are generated from ECsim and RelSIM, as described in Section 2.

Acknowledgments

N.R. was supported by the *ERC Advanced Grant TerraVirtualE* of Giovanni Lapenta (grant agreement No. 1101095310). Views and opinions expressed are however those of the authors only and do not necessarily reflect those of the European Union or the European Commission. Neither the European Union nor the European Commission can be held responsible for them. F.B. acknowledges support from the FED-tWIN programme (profile Prf-2020-004, project “ENERGY”) issued by BELSPO, and from the FWO Junior Research Project G020224N granted by the Research Foundation – Flanders (FWO). The resources and services used in this work were provided in part by the VSC (Flemish Supercomputer Center), funded by the Research Foundation - Flanders (FWO) and the Flemish Government. We acknowledge EuroCC Belgium for awarding this project access to the LUMI supercomputer, owned by the EuroHPC Joint Undertaking, hosted by CSC (Finland) and the LUMI consortium.

References

- Bacchini, F. (2023, oct). RelSIM: A Relativistic Semi-implicit Method for Particle-in-cell Simulations. *The Astrophysical Journal Supplement Series*, 268(2), 60. Retrieved from <https://dx.doi.org/10.3847/1538-4365/acefba> doi: 10.3847/1538-4365/acefba
- Birn, J., Artemyev, A. V., Baker, D. N., Echim, M., Hoshino, M., & Zelenyi, L. M. (2012, November). Particle Acceleration in the Magnetotail and Aurora. *Space Sci. Rev.*, 173(1-4), 49-102. doi: 10.1007/s11214-012-9874-4
- Burch, J. L., Moore, T. E., Torbert, R. B., & Giles, B. L. (2016, March). Magnetospheric Multiscale Overview and Science Objectives. *Space Sci. Rev.*, 199(1-4), 5-21. doi: 10.1007/s11214-015-0164-9
- Cohen, I. J., Turner, D. L., Mauk, B. H., Bingham, S. T., Blake, J. B., Fennell, J. F., & Burch, J. L. (2021). Characteristics of energetic electrons near active magnetotail reconnection sites: Statistical evidence for local energization. *Geophysical Research Letters*, 48(1), e2020GL090087.
- Dahlin, J. T. (2020). Adiabatic acceleration in a magnetotail flux rope. *Geophysical Research Letters*, 47(11), e2020GL087918. Retrieved from <https://agupubs.onlinelibrary.wiley.com/doi/abs/10.1029/2020GL087918> (e2020GL087918 10.1029/2020GL087918) doi: <https://doi.org/10.1029/2020GL087918>
- Dahlin, J. T., Drake, J. F., & Swisdak, M. (2017, 09). The role of three-dimensional transport in driving enhanced electron acceleration during magnetic reconnection. *Physics of Plasmas*, 24(9), 092110. Retrieved from <https://doi.org/10.1063/1.4986211> doi: 10.1063/1.4986211
- Ergun, R., Goodrich, K., Wilder, F., Ahmadi, N., Holmes, J., Eriksson, S., ... others (2018). Magnetic reconnection, turbulence, and particle acceleration: Observations in the earth’s magnetotail. *Geophysical Research Letters*, 45(8), 3338–3347.
- Ergun, R. E., Ahmadi, N., Kromyda, L., Schwartz, S. J., Chasapis, A., Hoilijoki, S., ... Burch, J. L. (2020, aug). Particle acceleration in strong turbulence in the earth’s magnetotail. *The Astrophysical Journal*, 898(2), 153. Retrieved from <https://dx.doi.org/10.3847/1538-4357/ab9ab5> doi:

- 10.3847/1538-4357/ab9ab5
- Genestreti, K. J., Nakamura, T. K. M., Nakamura, R., Denton, R. E., Torbert, R. B., Burch, J. L., ... Russell, C. T. (2018). How accurately can we measure the reconnection rate ϵ_m for the mms diffusion region event of 11 July 2017? *Journal of Geophysical Research: Space Physics*, 123(11), 9130-9149. Retrieved from <https://agupubs.onlinelibrary.wiley.com/doi/abs/10.1029/2018JA025711> doi: <https://doi.org/10.1029/2018JA025711>
- Guo, F., Li, H., Daughton, W., & Liu, Y.-H. (2014, Oct). Formation of hard power laws in the energetic particle spectra resulting from relativistic magnetic reconnection. *Phys. Rev. Lett.*, 113, 155005. Retrieved from <https://link.aps.org/doi/10.1103/PhysRevLett.113.155005> doi: 10.1103/PhysRevLett.113.155005
- Harris, E. (1962, 09). On a plasma sheet separating regions of oppositely directed magnetic field. *Il Nuovo Cimento*, 23, 115-121. doi: 10.1007/BF02733547
- Jokipii, J. R., Kota, J., & Giacalone, J. (1993, September). Perpendicular transport in 1- and 2-dimensional shock simulations. *Geophys. Res. Lett.*, 20(17), 1759-1761. doi: 10.1029/93GL01973
- Jones, F. C., Jokipii, J. R., & Baring, M. G. (1998, December). Charged-Particle Motion in Electromagnetic Fields Having at Least One Ignorable Spatial Coordinate. *Astrophys. J.*, 509(1), 238-243. doi: 10.1086/306480
- Lapenta, G. (2017). Exactly energy conserving semi-implicit particle in cell formulation. *Journal of Computational Physics*, 334, 349-366. Retrieved from <https://www.sciencedirect.com/science/article/pii/S0021999117300128> doi: <https://doi.org/10.1016/j.jcp.2017.01.002>
- Lapenta, G., Berchem, J., Alaoui, M. E., & Walker, R. (2020, Nov). Turbulent energization of electron power law tails during magnetic reconnection. *Phys. Rev. Lett.*, 125, 225101. Retrieved from <https://link.aps.org/doi/10.1103/PhysRevLett.125.225101> doi: 10.1103/PhysRevLett.125.225101
- Li, X., Guo, F., & Li, H. (2019, jun). Particle acceleration in kinetic simulations of nonrelativistic magnetic reconnection with different ion-electron mass ratios. *The Astrophysical Journal*, 879(1), 5. Retrieved from <https://dx.doi.org/10.3847/1538-4357/ab223b> doi: 10.3847/1538-4357/ab223b
- Li, X., Guo, F., Li, H., & Birn, J. (2018, mar). The roles of fluid compression and shear in electron energization during magnetic reconnection. *The Astrophysical Journal*, 855(2), 80. Retrieved from <https://dx.doi.org/10.3847/1538-4357/aaacd5> doi: 10.3847/1538-4357/aaacd5
- Li, X., Guo, F., Li, H., & Li, G. (2015, October). Nonthermally Dominated Electron Acceleration during Magnetic Reconnection in a Low- β Plasma. *Astrophys. Res. Letter*, 811(2), L24. doi: 10.1088/2041-8205/811/2/L24
- Li, X., Guo, F., Li, H., & Li, G. (2017, July). Particle Acceleration during Magnetic Reconnection in a Low-beta Plasma. *Astrophys. J.*, 843(1), 21. doi: 10.3847/1538-4357/aa745e
- Li, X., Guo, F., Li, H., Stanier, A., & Kilian, P. (2019, oct). Formation of power-law electron energy spectra in three-dimensional low- β magnetic reconnection. *The Astrophysical Journal*, 884(2), 118. Retrieved from <https://dx.doi.org/10.3847/1538-4357/ab4268> doi: 10.3847/1538-4357/ab4268
- Li, X., Guo, F., & Liu, Y.-H. (2021, 05). The acceleration of charged particles and formation of power-law energy spectra in nonrelativistic magnetic reconnection. *Physics of Plasmas*, 28(5), 052905. Retrieved from <https://doi.org/10.1063/5.0047644> doi: 10.1063/5.0047644
- Mauk, B. H., Blake, J. B., Baker, D. N., Clemmons, J. H., Reeves, G. D., Spence, H. E., ... Westlake, J. H. (2016a, March). The Energetic Particle Detector (EPD) Investigation and the Energetic Ion Spectrometer (EIS) for the Magnetospheric Multiscale (MMS) Mission. *Space Sci. Rev.*, 199(1-4), 471-514. doi: 10.1007/s11214-014-0055-5

- Mauk, B. H., Blake, J. B., Baker, D. N., Clemmons, J. H., Reeves, G. D., Spence, H. E., ... Westlake, J. H. (2016b, March). The Energetic Particle Detector (EPD) Investigation and the Energetic Ion Spectrometer (EIS) for the Magnetospheric Multiscale (MMS) Mission. *Space Sci. Rev.*, 199(1-4), 471-514. doi: 10.1007/s11214-014-0055-5
- Nakamura, R., Genestreti, K. J., Nakamura, T., Baumjohann, W., Varsani, A., Nagai, T., ... Torbert, R. B. (2019). Structure of the current sheet in the 11 July 2017 electron diffusion region event. *Journal of Geophysical Research: Space Physics*, 124(2), 1173-1186. Retrieved from <https://agupubs.onlinelibrary.wiley.com/doi/abs/10.1029/2018JA026028> doi: <https://doi.org/10.1029/2018JA026028>
- Nakamura, T. K. M., Genestreti, K. J., Liu, Y.-H., Nakamura, R., Teh, W.-L., Hasegawa, H., ... Giles, B. L. (2018). Measurement of the magnetic reconnection rate in the earth's magnetotail. *Journal of Geophysical Research: Space Physics*, 123(11), 9150-9168. Retrieved from <https://agupubs.onlinelibrary.wiley.com/doi/abs/10.1029/2018JA025713> doi: <https://doi.org/10.1029/2018JA025713>
- Northrop, T. G. (1963). Adiabatic charged-particle motion. *Reviews of Geophysics*, 1(3), 283-304. Retrieved from <https://agupubs.onlinelibrary.wiley.com/doi/abs/10.1029/RG001i003p00283> doi: <https://doi.org/10.1029/RG001i003p00283>
- Øieroset, M., Lin, R., Phan, T., Larson, D., & Bale, S. (2002). Evidence for electron acceleration up to 300 keV in the magnetic reconnection diffusion region of earth's magnetotail. *Physical Review Letters*, 89(19), 195001.
- Oka, M., Birn, J., Egedal, J., Guo, F., Ergun, R. E., Turner, D. L., ... Drake, J. F. (2023, December). Particle Acceleration by Magnetic Reconnection in Geospace. *Space Sci. Rev.*, 219(8), 75. doi: 10.1007/s11214-023-01011-8
- Oka, M., Phan, T. D., Øieroset, M., Turner, D. L., Drake, J. F., Li, X., ... Burch, J. L. (2022, 05). Electron energization and thermal to non-thermal energy partition during earth's magnetotail reconnection. *Physics of Plasmas*, 29(5), 052904. Retrieved from <https://doi.org/10.1063/5.0085647> doi: 10.1063/5.0085647
- Pollock, C., Moore, T., Jacques, A., Burch, J., Gliese, U., Saito, Y., ... Zeuch, M. (2016, March). Fast Plasma Investigation for Magnetospheric Multiscale. *Space Sci. Rev.*, 199(1-4), 331-406. doi: 10.1007/s11214-016-0245-4
- Rajhans, A., Oka, M., Øieroset, M., Phan, T., Cohen, I. J., Fuselier, S. A., ... Torbert, R. B. (2025). Energy partitioning between thermal and non-thermal electrons and ions in magnetotail reconnection. *Geophysical Research Letters*, 52(11), e2025GL114931. Retrieved from <https://agupubs.onlinelibrary.wiley.com/doi/abs/10.1029/2025GL114931> (e2025GL114931 2025GL114931) doi: <https://doi.org/10.1029/2025GL114931>
- Sironi, L., & Spitkovsky, A. (2014, feb). Relativistic reconnection: An efficient source of non-thermal particles. *The Astrophysical Journal Letters*, 783(1), L21. Retrieved from <https://dx.doi.org/10.1088/2041-8205/783/1/L21> doi: 10.1088/2041-8205/783/1/L21
- Torbert, R. B., Burch, J. L., Phan, T. D., Hesse, M., Argall, M. R., Shuster, J., ... Saito, Y. (2018). Electron-scale dynamics of the diffusion region during symmetric magnetic reconnection in space. *Science*, 362(6421), 1391-1395. Retrieved from <https://www.science.org/doi/abs/10.1126/science.aat2998> doi: 10.1126/science.aat2998
- Yamada, M., Kulsrud, R., & Ji, H. (2010, January). Magnetic reconnection. *Reviews of Modern Physics*, 82(1), 603-664. doi: 10.1103/RevModPhys.82.603
- Zhang, Q., Guo, F., Daughton, W., Li, H., & Li, X. (2021, Oct). Efficient nonthermal ion and electron acceleration enabled by the flux-rope kink instability in 3d nonrelativistic magnetic reconnection. *Phys. Rev. Lett.*, 127, 185101. Re-

trieved from <https://link.aps.org/doi/10.1103/PhysRevLett.127.185101>
doi: 10.1103/PhysRevLett.127.185101

Zhang, Q., Guo, F., Daughton, W., Li, X., & Li, H. (2024, oct). Plasma dynamics and nonthermal particle acceleration in 3d nonrelativistic magnetic reconnection. *The Astrophysical Journal*, 974(1), 47. Retrieved from <https://dx.doi.org/10.3847/1538-4357/ad6561> doi: 10.3847/1538-4357/ad6561